Available online at www.sciencedirect.com
SCIENCE DIRECT®

Journal of the European Ceramic Society 24 (2004) 2499–2507
www.elsevier.com/locate/jeurceramsoc

Influence of Nb^{5+} and Sb^{3+} dopants on the defect profile, PTCR effect and GBBL characteristics of $BaTiO_3$ ceramics

E. Brzozowski, M.S. Castro*

Institute of Materials Science and Technology (INTEMA) (Universidad Nacional de Mar del Plata—CONICET), Av. Juan B. Justo 4302, (B7608FDQ) Mar del Plata, Argentina

Received 24 June 2003; received in revised form 8 July 2003; accepted 19 July 2003

Abstract

In this work, a study of the electrical properties and defect structure of PTCR (positive temperature coefficient of resistance) and GBBL (grain boundary barrier layer) $BaTiO_3$-based ceramics was performed. For this study, different concentrations of Nb^{5+} or Sb^{3+} were employed for doping $BaTiO_3$. Based on the Heywang–Jonker model for PTCR materials, the density of acceptor states and the potential barrier height were calculated. Doping $BaTiO_3$ with small amounts of Nb_2O_5 led to higher potential barriers than those in Sb_2O_3-doped ceramics. From EPR analyses performed on the complete set of samples, paramagnetic defects were investigated. Hence, a relationship between the defect profile developed in the $BaTiO_3$ materials and the transition from a low resistivity to a high resistivity material was established. From this study, an increase in the titanium vacancies relative concentration along with an increment in the electrical resistivity measured at room temperature as the dopant content increases was confirmed.

Keywords: $BaTiO_3$ and titanates; Defects; Electrical properties; PTC devices

1. Introduction

Because of its large energy gap, chemically unmodified $BaTiO_3$ is an electrical insulator. However, barium titanate becomes a semiconducting material after the partial substitution of Ba^{2+} by trivalent cations, or Ti^{4+} by pentavalent cations.[1–3] In this case, conduction occurs through an electron-hopping mechanism.[4] Controlled incorporation of donor dopants in combination with an optimised ceramic process lead to PTCR (positive temperature coefficient of resistance) materials.[5,6] The PTCR effect in polycrystalline $BaTiO_3$ is characterised by a dramatic rise in the electrical resistivity across the tetragonal (ferroelectric) to cubic (paraelectric) transition around the Curie temperature (Tc).[7,8] Heywang[9] explained the PTCR effect in terms of double Schottky barriers at the grain boundaries. According to this model, these barriers result from electron trapping by acceptor states at the interfaces. Later on, Jonker[10–12] extended the model considering the influence of polarisation on the resistivity below the Curie point.

According to the Heywang model, the barrier height is given by:

$$e\phi(T) = e.N_e^2/(8.\varepsilon_o.\varepsilon_r.N), \quad (1)$$

where T is the absolute temperature (K), e the electron charge, ε_o is the dielectric constant of the free space, ε_r is the relative permittivity of the $BaTiO_3$, N the donor concentration and N_e the temperature dependent concentration of the occupied acceptor states.

Based on the Fermi–Dirac statistics, the next equation determines N_e:

$$N_e = N_s\ /(1 + \exp(E_F + e\phi(T) - E_s)/kT), \quad (2)$$

where $E_F = kT.\ln(N_C/N)$ is the Fermi level, N_s is the density of acceptor states, E_s is the energy of the surface state related to the bottom of the conduction band, k the Boltzmann constant, T the temperature,

* Corresponding author. Fax: +54-223-4810046.
E-mail addresses: ebrzozow@hotmail.com (E. Brzozowski), mcastro@fi.mdp.edu.ar (M.S. Castro).

0955-2219/$ - see front matter © 2003 Elsevier Ltd. All rights reserved.
doi:10.1016/j.jeurceramsoc.2003.07.015

$N_C = 1.56 \times 10^{28}$ m^{-3} the conduction electrons (the effective density of states, equal to the number of Ti ions per m^3).[12,13]

The effective resistivity of the sample follows the equation:

$$\rho_{eff} = \rho_g\,[1 + (b.k.T/d.e\phi(T)).\exp(e\phi(T)/kT)], \quad (3)$$

where $b = N_e/2N$ indicates the effective thickness of the grain boundary region, ρ_g is the grain resistivity, and d is the average grain size. The donor concentration (N) is related with the grain resistivity according to:

$$N = (\mu.e.\rho_g)^{-1}, \quad (4)$$

where μ is the electron mobility, and ρ_g the grain resistivity.

The barrier height is related with the measured dielectric constant as follows:

$$e\phi(T) = e.d.N_e/8.\varepsilon_o.\varepsilon_m, \quad (5)$$

where $\varepsilon_m = \varepsilon_r\,(d/2b)$ is the measured dielectric constant.

In the Heywang model, acceptor states arise from segregated impurities at the grain boundaries, whereas Jonker assumes that these surface states come from adsorbed oxygen.[11,12] On the other hand, studies by Daniels et al.[14,15] suggested that acceptor states are originated from barium vacancies. In tetragonal $BaTiO_3$, barium vacancies are neutral but above Tc, they trap electrons and become activated to singly ionised barium vacancies. Then, an electrically negative-charged region at the grain boundary and a positive space region adjacent to the boundaries are created, increasing the potential barrier. Since trapped electrons are not available for conduction, an increase in the electrical resistivity across the tetragonal-cubic transition of $BaTiO_3$ is observed.[16,17]

In this work, the effect of two dopants Nb^{5+} and Sb^{3+} on the defect profile and on the electrical properties of $BaTiO_3$-based materials was studied. Based on the Heywang–Jonker model for PTCR materials, the effect of these additives on the Schottky potential barriers at the grain boundaries in slightly-doped $BaTiO_3$ was analysed. A subsequent discussion concerning the electrical properties of highly-doped materials completed this work. In both cases, the relationship between the electrical response at room temperature and the charge compensation mode was established.

2. Experimental

Samples were prepared from commercial $BaTiO_3$ powders (TAM Ceramics Inc., Sr < 150 ppm as principal impurity, average grain size 0.84 μm, Ba/Ti = 1) and 0.05, 0.15 and 0.60 mol% of Nb_2O_5 (Fluka AG) or Sb_2O_3 (Aldrich). Starting powders were mixed by stirring in alcoholic medium with a high-speed turbine at 6000 rpm for 5 min. After drying, mixtures were crushed into powders and sieved through a 100 μm mesh screen. Finally, isostatically pressed cylinders (200 MPa) were sintered at 1350 °C for 2 h (heating and cooling rate: 3 °C/min). Table 1 summarises the characteristics of the studied samples.

In order to determine the average grain size (*d*), microstructures of the polished and thermally etched samples were analysed by SEM (Philips 505 microscope). X-ray diffraction (XRD) study of the $BaTiO_3$ samples was carried out on sintered samples, using a Philips PW 1050/25 equipment with CuK_α radiation and a Ni filter, at 40 KV and 30 mA. From the (002) and (200) diffraction profiles, a semi-quantitative study of the cell distortion was performed. To characterise the paramagnetic species in the crushed samples at room temperature, a Bruker ER-200D (Band X) EPR spectroscope with a gain of 2×10^4, a power of 5dB and modulation amplitude of 6.3Gpp was used. The EPR signal intensities were labelled as double integrated intensities (DII) calculated from the empirical relation reported by Murugaraj et al.:[17]

$$\begin{aligned} DII = &[(\text{signal height}).(\text{signal width})]/ \\ &[(\text{gain}).(\text{sample mass}).(\text{modulation amplitude}). \\ &(\text{power})^{1/2}], \end{aligned} \quad (6)$$

Table 1
Characteristics of the samples

Sample	Nb_2O_5 (mol%)	Sb_2O_3 (mol%)	*d* (μm)	Crystallographic system
P1	0.05	–	100	Tetragonal
P2	0.15	–	40	Pseudocubic
P3	0.60	–	2	Pseudocubic
P4	–	0.05	10	Tetragonal
P5	–	0.15	3	Pseudocubic
P6	–	0.60	2	Pseudocubic

Finally, for electrical measurements, samples were painted with a silver-palladium paste. All the electrical properties were measured from 20 to 160 °C by using the two-probe method. Electrical resistance was measured with an electrometer (Keithley 614) applying 0.01 V. The measured dielectric constant was calculated from the capacitance according to:

$$\varepsilon_m = C.t\ /(\varepsilon_o.S) \quad (7)$$

where C is the capacitance, t the thickness of the sample and S the area of the electrode. The capacitance was measured using a HP 4284A LCR analyser at 1 kHz. The grain-bulk resistivity of the different samples was taken from impedance analysis performed from room temperature to 400 °C in a Hewlett Packard (4192A-LF) analyser, using zero dc applied voltage, an amplitude of 1V and a 5 Hz–13 MHz frequency range.

3. Results

Fig. 1 shows the SEM images of the samples. In samples P1, P2, P4 and P5, a bimodal grain size distribution is observed. In these cases, grains of about 100 μm coexist with a fine-grained matrix (grain size about 1 μm). Exaggerated grain growth in modified $BaTiO_3$, is

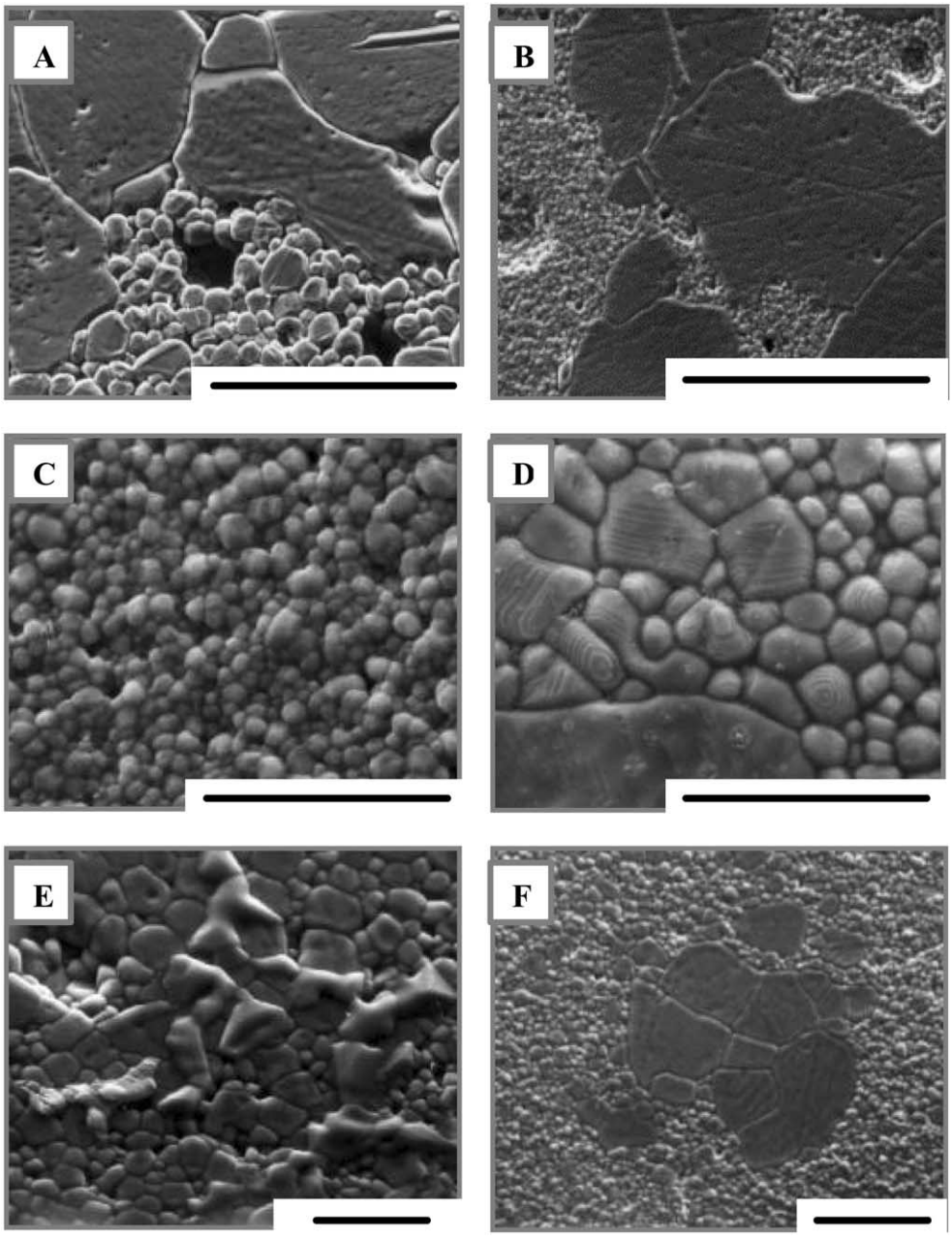

Fig. 1. SEM microphotographs of (A) P1, (B) P2, (C) P3, (D) P4, (E) P5 and (F) P6. Bar: 100 μm (A, B), 10 μm (C–F).

frequently associated to a non-uniform distribution of the dopant oxide in the $BaTiO_3$ powder.[18] Donor dopant restricts grain growth of $BaTiO_3$ at the sintering temperature and then, a strong inhibition of the grain growth in those dopant enriched regions is achieved. Samples with low dopant concentration heated for 2 h do not allow complete diffusion of dopants into pre-reacted $BaTiO_3$. However, it is possible to obtain homogeneous and completely fine-grained microstructures after doping with 0.60% of Nb_2O_5 (Fig. 1C, sample P3) or Sb_2O_3 (Fig. 1F, sample P6).

In Table 1, the average grain size (d) and the predominant crystallographic system are summarised. In fine-grained materials, the development of significant mechanical stresses in the grains lead to the stabilisation of a pseudocubic-structure.[7,8] Besides, symmetry of the diffraction peaks (Fig. 2) diminishes as the dopant content increased. According to Valot et al.,[19] symmetrical XRD signals result from the diffraction of ferroelectric domains. It is also worth noting that the "plateau" between these both peaks reported by the mentioned authors is a fingerprint of the mismatch among the domain walls in these ceramics.[19] On a similar way, Buscaglia et al. reported a diminution in the symmetry of the XRD peaks associated to the existence of at least two chemical and structural different regions within the grains of doped-$BaTiO_3$.[20] Therefore, seems to be a link between the incorporation of dopant and the evolution from a ferroelectric to a paraelectric structure in the Sb and Nb-doped samples studied here.

On the other hand, EPR analysis shows two kinds of paramagnetic signals at $g = 2.004$ and $g = 1.973$ and a weak signal at $g = 1.932$ in sample with antimonium addition. Murugaraj et al. assigned the EPR signal with giromagnetic constant $g = 1.997$ to barium vacancies (V_{Ba}') and the signal with $g = 1.963$, to singly ionised oxygen vacancies (V_O').[17] A recent article on $BaTiO_3$ defects related the EPR singlets with $g = 2.003$ and 1.973 to intrinsic point defects, V_{Ti} (probably V_{Ti}' or V_{Ti}''') and V_{Ba}', respectively.[21] Koodiazhnyi et al. reported an increment of the EPR intensity of both singlets at the Curie temperature in parallel with appearance of the PTCR effect.[21] Several authors observed the signal at $g = 1.932$ in n-semiconducting $BaTiO_3$ ceramics, which becomes negligible on further oxidation.[17,21] Based on the literature we assigned the signal with $g = 1.932$ to several Ti^{3+}-related paramagnetic defects, such as Ti^{3+}, $Ti^{3+}-V_o$, or $Ti^{3+}-V_o-K(Na)$.[21,22] Besides the mentioned singlets, a sextet lying at $g = 1.974$ was attributed to Mn^{2+} impurity in $BaTiO_3$.[17,21] The second EPR signal Table 2 shows the double integrated intensity of EPR signals (DII) corresponding to the mentioned species for each sample.

Samples P1, P2, P4 and P5 are blue in colour and exhibit a PTCR effect at the Curie temperature (Fig. 3). In these samples, curves of ε_r vs. T follow a Curie–Weiss

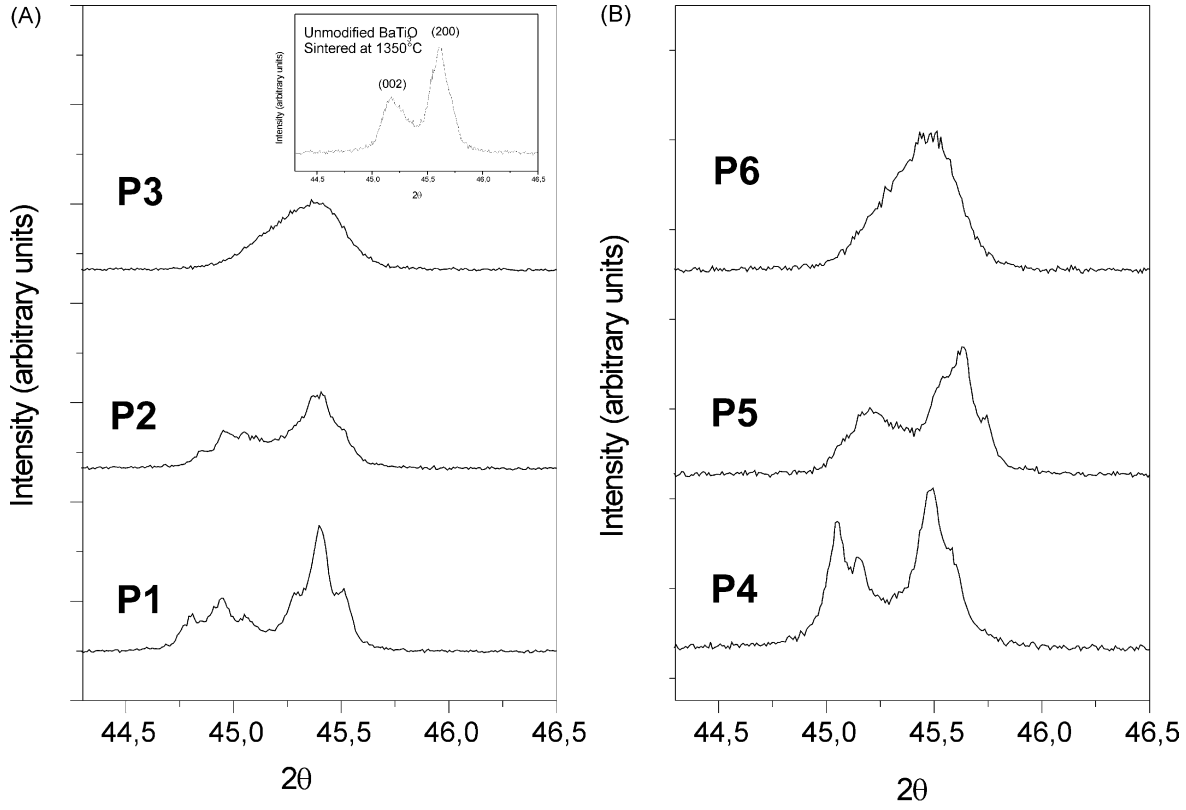

Fig. 2. XRD profiles of (A) Nb_2O_5 and (B) Sb_2O_3-doped $BaTiO_3$ sintered at 1350 °C for 2 h.

Table 2
Double integrated intensity (DII) of EPR signals for the samples at $g = 1.932$, $g = 1.973$ and $g = 2.004$

Sample	DII at $g = 1.963$	DII at $g = 1.973$	DII at $g = 2.004$
P1	–	<0.5	0.5
P2	–	<0.5	2
P3	–	<0.5	60
P4	2.1	6	0.5
P5	1.3	3.5	0.5
P6	1.3	4	3.5

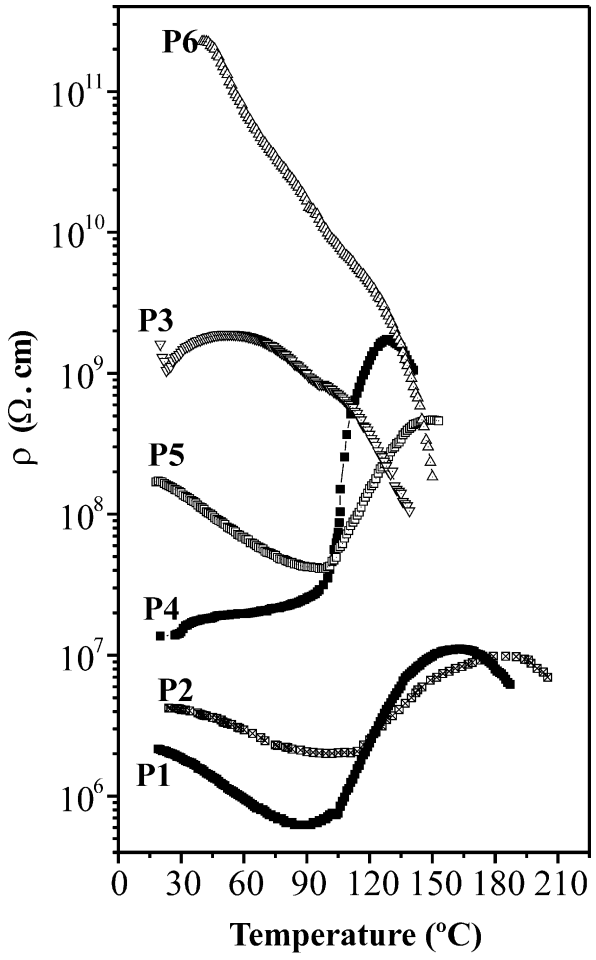

Fig. 3. Effective resistivity–temperature curves for Nb_2O_5 or Sb_2O_3-doped $BaTiO_3$.

behaviour, with a $T_c = 106$ and 102 °C for P1 and P2, respectively, while for P4 and P5 it is 96 °C (Fig. 4). On the other hand, highly-doped $BaTiO_3$ ceramics (P3 and P6) are yellow in colour and exhibit an extremely high resistivity ($\approx 10^{13}\Omega$.cm) at room temperature, with a NTCR effect as the temperature raises (Fig. 3). In the curves of ε_r vs. T (Fig. 5), at least two regions could be distinguished contributing with different T_c values. In these samples, the highest T_c value (T_{cmax}) yields on 102 °C (P3) or 94 °C (P6). The significant diminution in

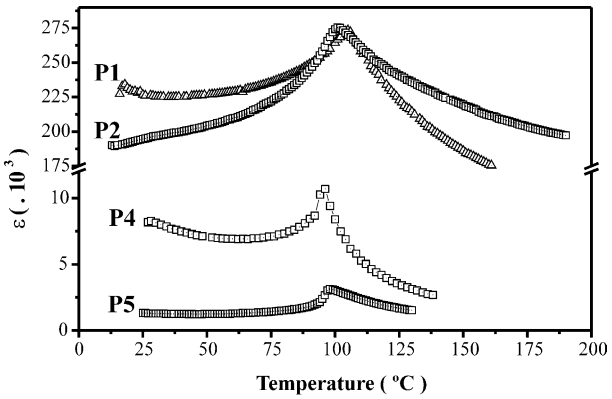

Fig. 4. Temperature dependence of the relative dielectric constant of samples P1, P2, P4 and P5.

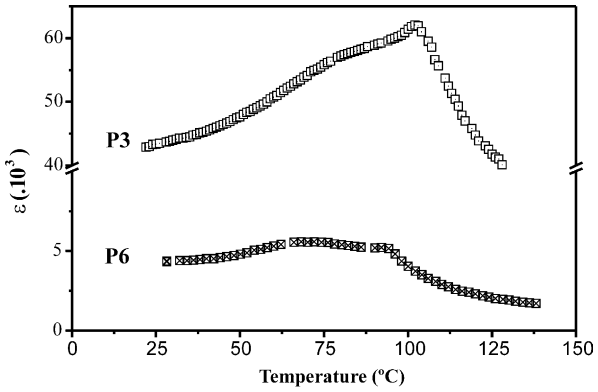

Fig. 5. Temperature dependence of the relative dielectric constant for samples P3 and P6.

the T_{cmax} registered in Sb_2O_3-doped material indicates higher dopant incorporation in this material than in Nb_2O_5–$BaTiO_3$ materials.

In the Heywang–Jonker model applied in PTCR ceramics, two parameters determined the barrier height at grain boundaries: the energy levels and the concentration of deep levels trapping electrons (N_s and E_s). These both parameters can be calculated from the resistivity–temperature curves and the Eqs. (1)–(5). Then, to determine the parameters of the Heywang–Jonker model (N_s, E_s, and e_ϕ) for the set of samples with PTCR effect, the iterative method reported in a previous paper[23] was employed. From the results, a good agreement between the experimental and calculated $\rho(T)$ curves for samples P1, P2, P4 and P5 is obtained. In Fig. 6A, experimental and calculated $\rho(T)$ vs. temperature curves for P1 are showed. Fig. 6B shows the calculated barrier height versus temperature curve for sample P1, while Fig. 6C shows the calculated Ns vs. temperature curve for this sample. For the other PTCR samples, well-matched experimental and calculated curves were also obtained (not showed here). Table 3 summarises the room-temperature parameters calculated for the PTCR samples (P1, P2, P4, P5).

4. Discussion

4.1. Dependence of the Heywang–Jonker parameters on dopant characteristics

As shown in Table 3, an increase in the density of acceptor states (Ns) and in the potential barrier height with the dopant content is observed. This tendency shows an important dependence with the dopant concentration. Considering the possible defects in $BaTiO_3$, the negative charge formed by titanium vacancies (V_{Ti}', V_{Ti}'', V_{Ti}''', V_{Ti}''''), barium vacancies (V_{Ba}', V_{Ba}'') and oxygen adsorbed, is compensated by a positive space region adjacent to the grain boundaries due to oxygen vacancies (V_O, $V_O^{\cdot\cdot}$), donor ions ($Sb_{Ba}^{\cdot}$, $Sb_{Ti}^{\cdot}$, or $Nb_{Ti}^{\cdot}$). In what follows, the influence of the additives on the defect concentration will be discussed.

Dopant concentration lead to different charge compensation mechanisms, as followed from EPR analyses. For low additive concentrations (0.05 – 0.15% mol) (see Table 2), vacancies formation is limited. In these cases, an electronic compensation regime prevails for both kinds of dopants, as it was proposed by Chan et al.[24,25] and Sasaki et al.:[26]

$$Nb_2O_5 + 2\ Ti_{Ti} \rightarrow 2Nb_{Ti}^{\cdot} + \frac{1}{2}\ O_2 + 2\ e' + 2TiO_2 \quad \text{(A)}$$

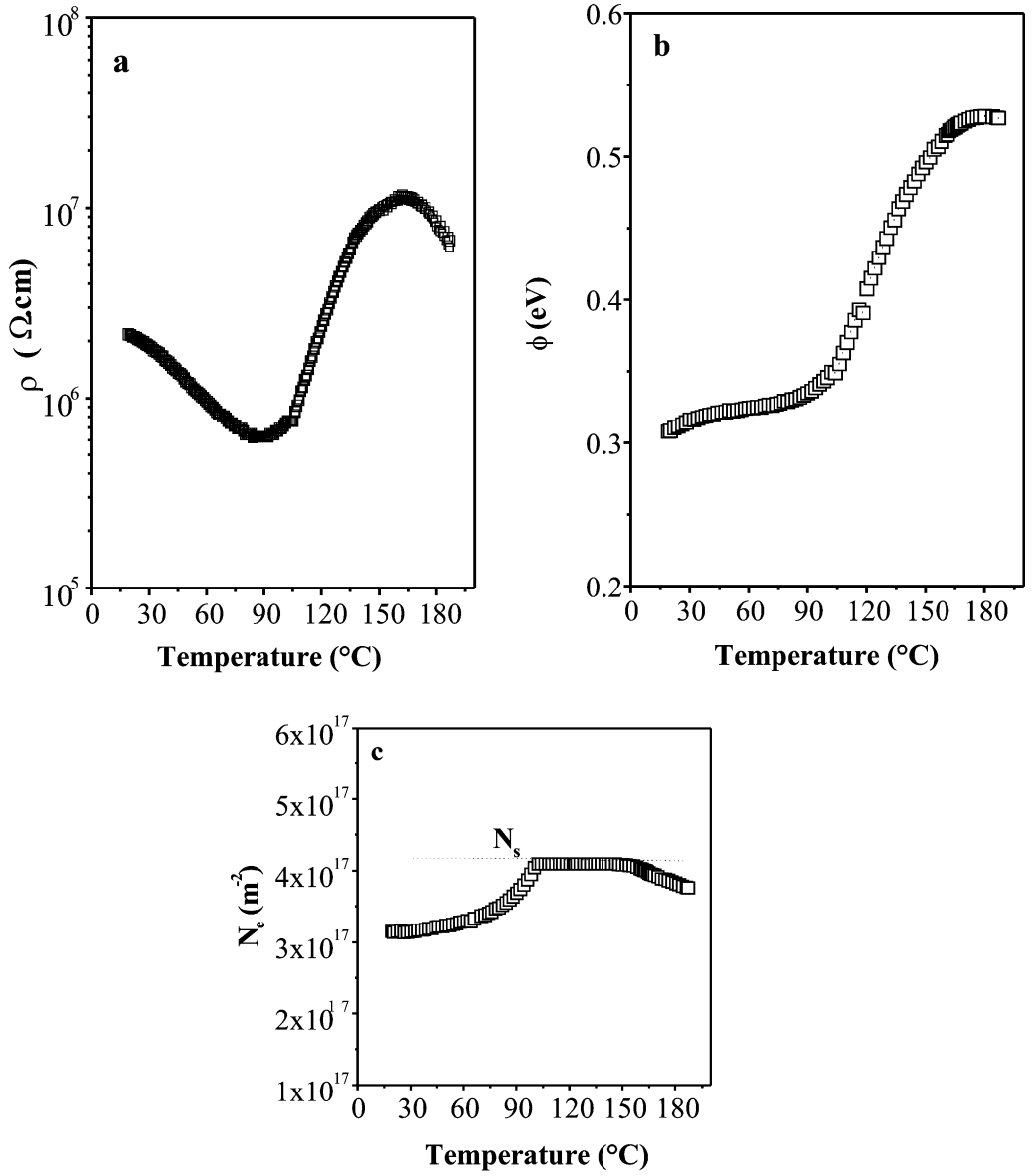

Fig. 6. Temperature dependence of the Heywang–Jonker parameters for sample P1; (a) Experimental and calculated $\rho(T)$—temperature curve (b) calculated $e\phi$—temperature curve (c) Calculated Ns—temperature curve.

$$Sb_2O_3 + 2\ Ba_{Ba} \rightarrow 2Sb^{\cdot}_{Ba} + \frac{1}{2}\ O_2 + 2\ e' + 2\ BaO \quad (B)$$

If a possible stabilisation of antimony as Sb_2O_5 is also considered:

$$Sb_2O_5 + 2Ti_{Ti} \rightarrow 2Sb^{\cdot}_{Ti} + \frac{1}{2}\ O_2 + 2e' + 2\ TiO_2 \quad (C)$$

In Eqs. (A)–(C), Nb^{5+}, Sb^{5+} and Sb^{3+} are donor dopants in the $BaTiO_3$ lattice replacing Ti^{4+} and Ba^{2+}, respectively. However, Sb^{3+} also acts as acceptor dopant when replaces Ti^{4+}. This phenomenon yields to a high concentration of double-ionised oxygen vacancies for the lowest dopant concentration (0.05% mol), as follows:

$$Sb_2O_3 + 2\ Ti_{Ti} + O_o \rightarrow 2Sb'_{Ti} + V^{\cdot\cdot}_{O} + 2\ TiO_2 \quad (D)$$

where double-ionised oxygen vacancies trap electrons according to

$$V^{\cdot\cdot}_{O} + 1e' \rightarrow V^{\cdot}_{O} \quad (E)$$

The following models proposed by Chan et al.[24,25] for Nb-doped $BaTiO_3$, and by Sasaki et al.[26] for Sb-doped $BaTiO_3$, represent the feasible mechanisms of compensation in those regions with high donor dopant contents:

$$Nb_2O_5 + 2\ Ti_{Ti} + Ba_{Ba} + 2\ O_o \rightarrow 2Nb^{\cdot}_{Ti} + V''_{Ba} + BaTiO_3 + TiO_2 \quad (F)$$

$$Sb_2O_3 + 3\ Ba_{Ba} \rightarrow 2Sb^{\cdot}_{Ba} + V''_{Ba} + 3\ BaO \quad (G)$$

$$Sb_2O_5 + 2Ti_{Ti} + Ba_{Ba} \rightarrow 2Sb^{\cdot}_{Ti} + V''_{Ba} + BaTiO_3 + TiO_2 \quad (H)$$

Double-ionised barium vacancies can transform into single ionised barium vacancies which is a paramagnetic specie:

$$V''_{Ba} + h \rightarrow V'_{Ba} \quad (I)$$

Generation of titanium vacancies (V_{Ti}'''') is other possible mechanism proposed for the ionic compensation regime:

$$2\ Nb_2O_5 + 5\ Ti_{Ti} \rightarrow 4Nb^{\cdot}_{Ti} + V''''_{Ti} + 5\ TiO_2 \quad (J)$$

$$2\ Sb_2O_3 + Ti_{Ti} + 4\ Ba_{Ba} \rightarrow 4Sb^{\cdot}_{Ba} + V''''_{Ti} + BaTiO_3 + 3\ BaO \quad (K)$$

$$2\ Sb_2O_5 + 5\ Ti_{Ti} \rightarrow 4Sb^{\cdot}_{Ti} + V''''_{Ti} + 5\ TiO_2 \quad (L)$$

The existence of this titanium vacancy doping mechanism was widely cited, although not universally accepted. According to Chiou and Lin,[27] titanium vacancies are unfavourable defects since its high effective charge provokes a charge disturbance not easy to compensate in the $BaTiO_3$ lattice. On the other hand, Chan et al.[24] reported that titanium vacancies generation are preferred defects for compensation of donor dopants. Recently, Morrison et al.[28] determined that a mechanism of titanium vacancy compensation is favoured at high donor doping. Buscaglia et al.[20] reported the formation of titanium vacancies for high-dopant concentrations. From our experimental observations by EPR a signal corresponding to titanium vacancies increases with the doping level.

A clear tendency to titanium vacancy formation with increasing dopant content is observed for either Nb or Sb–$BaTiO_3$ systems. The dramatic increase in titanium vacancy content for the 0.60% Nb_2O_5 doped $BaTiO_3$ material (Table 2) is a strong evidence of the importance of Eqs. (J)–(L) at high doping level. The rejection of Ti and/or Ba out of the grains is produced, modifying the electrical response of the material.

A less noticeable increase in barium vacancies after doping with Sb_2O_3 is observed, owing to the dual behaviour of Sb^{3+} as acceptor dopant [see Eq. (D)]. Oxygen vacancies compensate the partial acceptor behaviour of Sb^{3+} ions in Sb_2O_3 - doped materials. Due

Table 3
Heywang–Jonker parameters

Sample	N_s (cm^{-2})	N (cm^{-3})	ρ_g (Ω.cm)	E_s (eV)	$e\phi$ (eV)	
					298 K	478 K
P1	4.1×10^{13}	1.237×10^{16}	1.010×10^{3}	1.18	0.31	0.43
P2	2.861×10^{14}	2.0×10^{17}	33	1.41	0.53	0.66
P4	3.01×10^{11}	1.375×10^{12}	9.1×10^{6}	0.8	<0.1	
P5	5.96×10^{12}	4.16×10^{14}	2.710×10^{4}	1.2	0.21	0.32

to the dual behaviour of Sb^{3+}, the actual donor concentration is lower than the nominal concentration and a charge compensation mechanism by oxygen vacancies (V_O) can also appear (see Table 2). Therefore, the low N_s values and the extremely low potential barriers at the grain boundaries of Sb_2O_3-doped samples reflect this phenomenon.

4.2. Relationship between ρ_g and an electronic charge compensation mechanism in the grain bulk

As it is shown in Table 3, the grain bulk resistivity diminishes as the nominal doant concentration increases. According to Desu et al.,[29–33] for slightly doped $BaTiO_3$ the electron concentration increases linearly with the donor content until a critical concentration of dopant is reached. At high donor concentration, there is a shift from the electronic to an ionic vacancy compensation regime. In this work, this phenomenon could also be present along each grain with a gradual change in chemical, structural and electrical characteristics toward the grain bulk. This effect obeys to a differential dopant distribution along the $BaTiO_3$ grains leading to regions with different electrical properties, as it is evidenced by the dielectric constant-temperature curves (Figs. 4 and 5). In these materials, a transition from the electron compensation to vacancy compensation along each grain occurs. Slightly-doped $BaTiO_3$ (electronically compensated) prevails in the grain core leading to a low-resistive grain bulk.

In Sb_2O_3-doped materials, the additional acceptor behaviour of Sb^{3+} ions contributes to a further increase of ρ_g as oxygen vacancies are created.

4.3. Microstructure characteristics and effective electrical resistivity of Nb_2O_5 and Sb_2O_3-doped $BaTiO_3$

Despite the Sb_2O_3-doped materials showed low potential barriers at room-temperature (Table 3), the effective resistivity values are significantly high (Fig. 3). Desu et al[32,33] calculated the effective resistivity considering the influence of the insulating region resistivity (ρ_i) and the thickness of the insulating region (l_i) on the effective grain resistivity (ρ_{effg}):

$$\rho_{eff} = \rho_{effg} + l_i \,.\rho_i / \, R_2 \tag{8}$$

where R_2 is the grain radio.

It is assumed that the insulating region is built due to donor segregation phenomena. Because the ionic radius misfit in Ba^{2+} (0.134 nm)[34]/Sb^{3+} (0.076 nm),[34] Ti^{4+} (0.068 nm)[34]/Sb^{3+} (0.076 nm),[34] and Ti^{4+} (0.068 nm)[34]/Sb^{5+} (0.062 nm)[34] couples is higher than it in the Ti^{4+} (0.068 nm)[34]/Nb^{5+} (0.069 nm)[34] couple, the tendency of Sb^{3+} to segregate out of the $BaTiO_3$ lattice is higher. Sb^{3+} replaces Ba^{2+} and Ti^{4+} till the solubility limit is reached, then Sb^{3+} impurities are accumulated at the grain boundaries, leading to the insulating region. In samples P4, P5 and P6, high Sb^{3+} incorporation and subsequent segregation at the grain boundaries lead to an enhanced insulating region. In addition to it, dopant segregation and vacancies formation pin grain boundaries mobility during sintering, inhibiting grain growth. As the effective electrical resistivity for PTCR-$BaTiO_3$ also depends on the density of grain boundaries in the total sample,[12,13] The effective conductivity of the materials with a fine-grained matrix (P2, P3, P5, P6) is strongly reduced.

In this work, barium titanate-based materials revert to an insulating behaviour after doping with the highest concentration of Nb_2O_5 or Sb_2O_3 (0.60% mol). Considering the formation of resistive grain boundary layers, Desu and Payne explained the semiconducting-insulating transition in doped-$BaTiO_3$.[33] These authors assumed an n-i-n structure at the grain boundaries of $BaTiO_3$. According to these authors, high-resistivity values in GBBL materials depend on the relative thickness of the grain-boundary insulating layer, the space charge layer and the grain size. In the fine-grained materials studied in this work, results indicate a thick insulating layer at the grain boundaries against a very thin space charge layer. Consequently, polarisation in the grain bulk is not high enough to decrease the potential barriers at the grain boundaries.

5. Conclusions

The addition of small amounts of Nb_2O_5 or Sb_2O_3 to $BaTiO_3$ with lead to relatively low resistivity at room temperature and a PTCR effect at the Curie temperature.

In PTCR materials, a relationship between barium and titanium vacancy concentration and high Schottky barriers at grain boundaries was found. These results support the hypothesis of the apparition of a negatively layer at the grain boundaries due to the presence of barium and titanium vacancies and oxygen species. This layer is compensated by a positively charged region adjacent to the grain boundary. This region is mainly composed by oxygen vacancies and substitutional ions.

In $BaTiO_3$ doped with small amounts of Nb_2O_5, higher potential barriers than those in Sb_2O_3-doped ceramics are obtained. This phenomenon is associated to the donor character of Nb^{5+}. In Sb_2O_3 doping, an additional incorporation of Sb^{3+} as acceptor in the Ti sublattice led to oxygen vacancies creation mechanism in detriment of the electron generation regime.

High dopant concentrations lead to a GBBL behaviour in $BaTiO_3$ ceramics doped with Nb_2O_5 or Sb_2O_3. In these materials, a thick layer rich in barium vacancies at the grain boundaries governs the effective resistivity of the ceramics.

Acknowledgements

Authors acknowledge the Fundación Antorchas, CONICET and Universidad Nacional de Mar del Plata for financial support.

References

1. Chiou, B. S. and Warng, I. H., Effect of MgO addition on the electrical transport properties of highly Sb-doped $BaTiO_3$ ceramics. *J. Mat. Sci.: Mat. in Electron*., 1998, **9**, 145–150.
2. Hozer, L. Positive temperature coefficient of resistivity (PTCR) thermistors. In *Semiconductor Ceramics, Grain Boundary Effects*, Ellis Horwood Series in Physics and its applications, Poland, (1994) pp. 109–147.
3. Urek, S., Drofenik, M. and Makovec, D., Sintering and properties of highly donor-doped barium titanate ceramics. *J. Mat. Sci*., 2000, **35**, 895–901.
4. LaCourse, B. C. and Amarakoon, V. R. W., Characterization of the firing schedule for positive temperature coefficient of resistance $BaTiO_3$. *J. Am. Ceram. Soc*., 1995, **78**, 3352–3356.
5. Drofenik, M., Makovec, D., Zajc, I. and Lanhmmer, H. T., Anomalous grain growth in donor-doped barium titanate with excess of barium oxide. *J. Am. Ceram. Soc*., 2002, **85**, 653–660.
6. Ramajo, M., Brzozowski, E. and Castro, M. S., Estudio del perfil de defectos y de la propiedades eléctricas de $BaTiO_3$ dopado con Nb y La. *Bol. Soc. Esp. Cer. Vidrio*, 2002, **41**, 31–35.
7. Kuwabara, M. and Matsud, H., Shift of the Curie point of barium titanate ceramics with sintering temperature. *J. Am. Ceram. Soc*., 1997, **80**, 2590–2596.
8. Begg, B. D., Vance, E. R., Cassidy, D. J., Nowotny, J. and Blairs, S., Particle size effect on the room temperature structure of barium titanate. In *Grain Boundaries and Interfaces in Electronic Ceramics, Ceramics Transactions, Vol. 41*, ed. L. M. Levinson and S. Hirano, 1994, pp. 169–176.
9. Heywang, W., Resistivity anomaly in doped $BaTiO_3$. *J. Am. Ceram. Soc*., 1964, **47**, 484–490.
10. Nowotny, J. and Rekas, M., Positive temperature coefficient of resistivity for $BaTiO_3$ based materials. *Ceram. Int*., 1991, **17**, 227–241.
11. Jonker, G. H., Halogen Treatment of barium titanate semiconductors. *Mat. Res. Bull*., 1967, **2**, 401–407.
12. Jonker, G. H., Some aspects of semiconducting barium titanate. *Solid State Electron*., 1964, **7**, 895–903.
13. Issa, M. A. A., Electrical properties of polycrystalline PTCR barium titanate. *J. Mat. Sci*., 1992, **27**, 3685–3692.
14. Daniels, J. and Wernicke, R., Part V. News aspects for an improved PTCR model. *Philips Res. Rept*., 1976, **31**, 544–559.
15. Daniels, J., Hardtl, K. H. and Wernicke, R., The PTC effect of barium titanate. *Philips Tech. Rev*., 1979, **38**, 73–82.
16. Murugaraj, P. and Kutty, T. R. N., EPR study of the Fe^{3+} ion influence on the PTCR of $BaTiO_3$. *J. Mat. Sci. Lett*., 1986, **5**, 171–173.
17. Murugaraj, P., Kutty, T. R. N. and Subba Rao, M., Diffuse phase transformations in neodymium - doped $BaTiO_3$ ceramics. *J. Mater. Sci*., 1986, **21**, 3521–3527.
18. Brzozowski, E., Castro, M. S., Foschini, C. R. and Stojanovic, B., Secondary phases in Nb-doped $BaTiO_3$ ceramics. *Ceram. Int*., 2002, **28**, 773–777.
19. Valot, C. M., Floquet, N. and Niepce, J. C., Microstructure of 90° domains in ferroelectric materials studied by XRD. *Key Eng. Mat*., 1997, **132–136**, 1127–1130.
20. Buscaglia, M. T., Buscaglia, V., Viviani, M., Nanni, P. and Hanuskova, M., Influence of foreign ions on the crystal structure of $BaTiO_3$. *J. Eur. Ceram. Soc*., 2000, **20**, 1997–2007.
21. Kolodiazhnyi, T. and Petric, A., Analysis of point defects in polycrystalline $BaTiO_3$ by electron paramagnetic resonance. *J. Phys. Chem. Solids*, 2003, **64**, 953–966.
22. Scharfschwerdt, R., Mazur, A., Schimer, O. F., Hesse, H. and Mendricks, S., Oxygen vacancies in $BaTiO_3$. *Phys. Rev. B*, 1996, **54**, 15284–15290.
23. Brzozowski, E. and Castro, M. S., Conduction mechanism of barium titanate ceramics. *Ceram. Int*., 2000, **26**, 265–269.
24. Chan, H. M., Harmer, M. and Smyth, D. M., Compensating defects in highly donor-doped $BaTiO_3$. *J. Am. Ceram. Soc*., 1986, **69**, 507–510.
25. Chan, N.-H. and Smyth, D. M., Defect chemistry of donor-doped $BaTiO_3$. *J. Am. Ceram. Soc., Discussions and Notes*, 1972, **67**, 285–288.
26. Sasaki, Y., Fujii, I., Matsui, T. and Morii, K., Influence of antimony doping on electrical properties of barium titanate ($BaTiO_3$) thin films. *Mat. Lett*., 1996, **26**, 265–271.
27. Chiou, B.-S. and Lin, S.-T., EPR evidence for compensating defects in $BaTiO_3$ grain boundary barrier layer capacitors. *Mat. Chem. Phys*., 1990, **24**, 239–245.
28. Morrison, F. D., Sinclair, D. C. and West, A. R., An altenative explanation for the origin of the resistivity anomaly in La-doped $BaTiO_3$. *J. Am. Ceram. Soc*., 2001, **84**, 474–476.
29. Desu, S. B. and Payne, D. A., Interfacial effects in perovskites. *Key Eng. Mat*., 1992, **66/67**, 375–420.
30. Desu, S. B. and Payne, D. A., Interfacial segregation in perovskites: I, theory. *J. Am. Ceram. Soc*., 1990, **73**, 3391–3397.
31. Desu, S. B. and Payne, D. A., Interfacial segregation in Perovskites: II, experimental evidence. *J. Am. Ceram. Soc*., 1990, **73**, 3398–3406.
32. Desu, S. B. and Payne, D. A., Interfacial segregation in Perovskites: III, microstructure and electrical properties. *J. Am. Ceram. Soc*., 1990, **73**, 3407–3415.
33. Desu, S. B. and Payne, D. A., Interfacial segregation in perovskites: IV, internal boundary layer devices. *J. Am. Ceram. Soc*., 1990, **73**, 3416–3421.
34. Shannon, R. D., Revised effective ionic radii in halides and chalcogenides. *Acta Cryst. A*, 1976, **32**, 751.